ROLL PREDICTION AND PARAMETER IDENTIFICATION OF MARINE VESSELS UNDER UNKNOWN OCEAN DISTURBANCES

Sang-Do Lee
Division of Navigation & Information System, Mokpo National Maritime University, Republic of Korea
Hwan-Seong Kim*
Division of Logistics, Korea Maritime and Ocean University, Republic of Korea
Sam-Sang You
Northeast-Asia Shipping and Port Logistics Research Center, Korea Maritime and Ocean University, Republic of Korea
Jeong-Hum Yeon
R&D Department, Busan Port Authority, Republic of Korea
Bui Duc Hong Phuc
Department of Engineering Technology, Gadomski School of Engineering, Christian Brothers University, United States

* Corresponding author: *kimhsyskmou@gmail.com (Hwan-Seong Kim)*

ABSTRACT

This paper deals with two topics: roll predictions of marine vessels with machine-learning methods and parameter estimation of unknown ocean disturbances when the amplitude, frequency, offset, and phase are difficult to estimate. This paper aims to prevent the risky roll motions of marine vessels exposed to harsh circumstances. First of all, this study demonstrates complex dynamic phenomena by utilising a bifurcation diagram, Lyapunov exponents, and a Poincare section. Without any observers, an adaptive identification applies these four parameters to the globally exponential convergence using linear second-order filters and parameter estimation errors. Then, a backstepping controller is employed to make an exponential convergence of the state variables to zero. Finally, this work presents the prediction of roll motion using reservoir computing (RC). As a result, the RC process shows good performance for chaotic time series prediction in future states. Thus, the poor predictability of Lyapunov exponents may be overcome to a certain extent, with the help of machine learning. Numerical simulations validate the dynamic behaviour and the efficacy of the proposed scheme.

Keywords: Non-periodic roll motions, dynamic analysis, reservoir-computing, parameter estimation, periodic disturbances, backstepping

INTRODUCTION

Marine vessels frequently encounter roll behaviour. Non-periodic patterns appear at the end of stable responses, despite regular waves. This phenomenon is hard to predict and control by the officers on the bridge. Chaos is an aperiodic, long-term motion that exhibits sensitive dependence on initial conditions in a deterministic system. Even slight changes in initial conditions (IC) result in various outcomes. The sensitivity of a chaotic dynamic system has merit because it shows a different periodic orbit by using a light adjustment of parameters without the whole reconstruction of the system [1]. However, controlling the non-periodic behaviour of a chaotic system is not a trivial issue in the marine environment.

First of all, this paper attempts to predict non-periodic roll motions through machine learning (ML) techniques,

before their manipulation. Simple and complex systems were recently studied under a veil of chaos, using ML, to contribute to predicting dynamic behaviour [2]. Notably, echo state networks (ESN), which are termed 'reservoir computing' (RC), are efficient and easy to apply to the black box modelling of dynamic systems [3]. The RC is a recurrent neural network (RNN)-based framework that enables the readout to extract the desired output by using linear mapping [4, 5]. The sensitivity of a chaotic system challenges prediction, which only works if the initial uncertainty is not quickly multiplied by the evolution law [6]. However, this skill is preferable for chaotic time series forecasts because it remembers past values and handles external disturbances, where all of the past elements are implicitly contained in a state vector [4].

As mentioned, the non-periodic roll motions are revealed at the end of stable responses, despite regular excitations [7]. However, estimating the frequencies of unknown external disturbances is difficult because the waves acting on a ship can not be known in advance [8]. Under manoeuvring conditions, it is difficult to measure the exact amounts of time-varying disturbances for a ship, such as waves, winds, currents, ice-covered waters, green waters, etc. Also, estimating the sinusoidal signal is a significant problem for the control system. It is essential to identify the parameters of unknown periodical excitations in tracking and rejection control [9]. In order to realise the safe voyage of marine vessels under severe sea situations, this paper investigates the parameter estimation of unknown periodic disturbances and the suppression of non-periodic roll motions.

It is known that a periodic excitation consists of the sum of its frequency, amplitude, bias (offset), and phase (randomness). As for the real-time processing of chaotic motion in nonlinear systems, a potential solution, based on Fourier analysis, is deemed to be an unwelcome method, owing to the maximisation of the periodogram [10]. A similar work [10] identified the full parameters by using a fifth-order estimator, showing the complexity and computational costs. The frequency and other parameter estimation techniques are separated in the present paper. Other parameter estimations of amplitude, bias, and phase are treated using the simple update law without any observers [9, 11]. In order to design the disturbance rejection control, precise frequency estimation is guaranteed with finite-time convergence [8]. To achieve the stability and robustness of a nonlinear system, this paper implements linear second-order filters and parameter estimation errors, to converge the global parameter estimation without a higher-order estimator. Such a filtering operation overcomes the infinitely increasing auxiliary vector [12]. Then, a backstepping control is designed to suppress the non-periodic roll motions of the marine vessels under unknown periodic disturbances.

The remainder of the paper is organised as follows. A ship rolling model and control synthesis for non-periodic roll stabilisation, using backstepping and roll prediction with RC, are explained in Section 2. The parametric estimation of amplitude, frequency, offset, phase, and adaptive mechanisms is expressed. Numerical simulations verify the proposed schemes in Section 3. The dynamic theory is used to explore the uncontrolled roll responses using the bifurcation diagram, Poincare map, and Lyapunov exponents (LEs). Final remarks and recommended future research directions are given in Section 4.

MATHEMATICAL FORMULATION

SHIP ROLLING MODEL

The rolling motion of a ship, in transverse directions, can be modelled as follows [7]:

$$\left[I_{44} + A_{44} \right] \ddot{\phi} + B_{44} \dot{\phi} + \Delta \overline{GZ}(\phi) = F_{sea}(t) \quad \text{(1)}$$

where ϕ (rad), $\dot{\phi}$ (rad/s), and $\ddot{\phi}$ (rad/s²) are the roll angle, rate, and acceleration; I_{44}, and A_{44} (kg·m^2) are the moment of inertia and the added mass coefficients; and B_{44} (kg·m^2/s) is the damping coefficient. It should be noted that both the added mass and hydrodynamic damping coefficients are a function of the wave frequency; Δ is the ship's displacement; $\overline{GZ}$ is the righting lever; and F_{sea} is the wave-exciting moment. As for periodic roll excitation, the external wave F_{sea} is given as:

$$F_{sea}(t) = HF_{roll}(\omega)\cos(\omega t) \quad \text{(2)}$$

where F_{roll} (N·m) is the rolling moment; and ω and H are the angular frequency and the wave amplitude. Generally, Eq. (1) can be rewritten with a quadratic damping, as follows:

$$\left[I_{44} + A_{44} \right] \ddot{\phi}(t) + B_{44} \dot{\phi}(t) + B_{44q} \dot{\phi}(t)\left|\dot{\phi}(t)\right| - C_1 \Delta \phi(t)$$
$$+ C_3 \Delta \phi^3(t) = HF_{roll}(\omega)\cos(\omega t) \quad \text{(3)}$$

where B_{44q} is the quadratic damping coefficient. Eq. (3) can be scaled into a non-dimensional equation, thus:

$$\frac{\omega_n^2(I_{44} + A_{44})}{C_1 \Delta} \ddot{x}(\tau) + \frac{\omega_n B_{44}}{C_1 \Delta} \dot{x}(\tau) + \frac{\omega_n^2 B_{44q}}{C_1 \Delta} \dot{x}(\tau)\left|\dot{x}(\tau)\right|$$
$$- x(\tau) + \frac{C_3}{C_1} x^3(\tau) = \frac{HF_{roll}(\omega)}{C_1 \Delta} \cos(\Omega\tau) \quad \text{(4)}$$

with $x(\tau) = \phi(t)$, $\tau = \omega_n t$, and $\Omega = \omega / \omega_n$; where Ω is the ratio of excitation (ω) to a natural angular frequency (ω_n). Then, the simplified form is derived as:

$$\ddot{x}(\tau) + b_1 \dot{x}(\tau) + b_2 \dot{x}(\tau)\left|\dot{x}(\tau)\right| - x(\tau) + kx^3(\tau) = F\cos(\Omega\tau) \quad \text{(5)}$$

with

$$b_1 = \frac{B_{44}}{\omega_n(I_{44} + A_{44})} = \frac{\omega_n B_{44}}{C_1\Delta}, \quad \omega_n = \sqrt{\frac{C_1\Delta}{I_{44} + A_{44}}}$$

$$b_2 = \frac{B_{44q}}{I_{44} + A_{44}}, \quad k = \frac{C_3}{C_1}, \quad F = \frac{HF_{roll}}{\omega_n^2(I_{44} + A_{44})} = \frac{HF_{roll}}{C_1\Delta}$$

where b_1 and b_2 are the linear and nonlinear damping and k is the restoring part of a duffing type roll motion.

CONTROL SYNTHESIS OF BACKSTEPPING

The idea of backstepping is to recursively design a controller by considering some of the state variables as being 'virtual controls' and creating intermediate control laws for them [13]. This method is one of the proper nonlinear controllers for regulating the desired ship motions. By adding the actuation (u) in Eq. (5), the complete control system represents a forced rolling system with an active control input:

$$\ddot{x} + b_1\dot{x} + b_2\dot{x}|\dot{x}| - x + kx^3 = F\cos(\Omega\tau) + u \quad \text{(6)}$$

where the periodic excitation $F\cos(\Omega\tau)$ is given as a time-varying disturbance. In fact, an active controller is vital, to achieve a satisfactory anti-rolling effect. By selecting the state variables as $x = x_1$ and $\dot{x} = x_2$, the governing Eq. (6) can be rewritten into the state-space representation, as follows:

$$\dot{x} = Ax + f(x,\tau) + Bu + B_1 d \quad \text{(7)}$$

In Eq. (7), d represents the time-varying disturbance input ($F\cos(\Omega\tau)$), while the state vector (x), system matrices (A, B, B_1), and nonlinear term (f) are described by:

$$x = \begin{bmatrix} x_1 \\ x_2 \end{bmatrix}, A = \begin{bmatrix} 0 & 1 \\ 1 & -b_1 \end{bmatrix},$$

$$B = B_1 = \begin{bmatrix} 0 \\ 1 \end{bmatrix}, f(x,\tau) = \begin{bmatrix} 0 \\ -b_2 x_2|x_2| - kx_1^3 \end{bmatrix} \quad \text{(8)}$$

In the dynamic model, there are two types of *inputs*: the control (u), which can be manipulated by the control actuator, and the *disturbance* (d), which represents external influences on ship motion. The two state variables are rewritten in the state-space representation form,

$$\begin{cases} \dot{x}_1 = x_2 \\ \dot{x}_2 = x_1 - b_1 x_2 - b_2 x_2|x_2| - kx_1^3 + d + u \end{cases} \quad \text{(9)}$$

From Eq. (9), x_2 is considered to be a virtual control input for x_1. To make x_1 exponentially converge to zero, the desired value for x_2 is chosen at $x_{2d} = -\gamma_1 x_1$, where γ_1 is a positive constant. Consequently, $x_2 \rightarrow x_{2d}$ would yield the solution $x_1 \rightarrow x_{1d} = x_1(0)e^{-\gamma_1 t}$. We declare $z_2 = x_2 - x_{2d} = x_2 + \gamma_1 x_1$ as the tracking error of state x_2 and define a positive definite (P.D.) The Lyapunov function is as follows:

$$V_1 = \frac{1}{2}x_1^2 + \frac{1}{2}z_2^2 \quad \text{(10)}$$

Then the derivative of V_1 is given as:

$$\dot{V}_1 = x_1\dot{x}_1 + z_2\dot{z}_2 = -\gamma_1 x_1^2$$
$$+ z_2(2x_1 + \gamma_1 x_2 - b_1 x_2 - b_2 x_2|x_2| - kx_1^3 + d + u) \quad \text{(11)}$$

As z_2 should be asymptotically stable, $\dot{V}_1$ is expected to be a negative definite (N.D.) function. If the disturbance is well-defined, the control input can be given as follows:

$$u(t) = -2x_1 - \gamma_1 x_2 + b_1 x_2 + b_2 x_2|x_2| + kx_1^3 - d - \gamma_2 z_2 \quad \text{(12)}$$

where γ_2 is a positive constant, resulting in a P.D. function $\dot{V}_1 = -\gamma_1 x_1^2 - \gamma_2 z_2^2$. However, since the amplitude and frequency of disturbance are hardly recognised, the control input cannot be defined as Eq. (12). In fact, the control input is dependent on the estimated value $\hat{d}$ instead of d, so the controller in Eq. (12) should be rewritten as:

$$u(t) = -2x_1 - \gamma_1 x_2 + b_1 x_2 + b_2 x_2|x_2| + kx_1^3 - \hat{d} - \gamma_2 z_2 \quad \text{(13)}$$

which would yield

$$\dot{V}_1 = -\gamma_1 x_1^2 - \gamma_2 z_2^2 + z_2(d - \hat{d}) \quad \text{(14)}$$

The problem is to make an estimation $\hat{d}$ that eliminates the term $z_2(d - \hat{d})$. In general, four critical features should be determined, to define a sinusoidal signal completely, in terms of offset, amplitude, frequency, and phase. Assuming that $\hat{d}(\tau) = \hat{F}_o + \hat{a}\cos(\hat{\Omega}\tau) + \hat{b}\sin(\hat{\Omega}\tau)$, where $\hat{F}_o$ is the estimated offset, $\hat{\Omega}$ is the estimated frequency, $\hat{F} = \sqrt{\hat{a}^2 + \hat{b}^2}$ is the estimated amplitude, and $\hat{\psi} = \arctan(\hat{b}/\hat{a})$ is the estimated phase. The following subsections will present an adaptive mechanism to update those components.

ESTIMATION FOR FREQUENCY

Let us introduce a second-order filter for the disturbance, as shown in Eq. (15),

$$\xi(s) = \frac{\lambda_0}{s^2 + \lambda_1 s + \lambda_2} d(s) \tag{15}$$

where $\lambda_0, \lambda_1,$ and λ_2 are positive constants that make $\Lambda(s) = s^2 + \lambda_1 s + \lambda_2$ a Hurwitz polynomial. Neglecting the initial conditions, it is simple to obtain the relation as follows:

$$\dddot{\xi}(t) = -\Omega^2 \dot{\xi}(t) = \Theta \dot{\xi}(t) + \varepsilon_\xi(t) \tag{16}$$

where $\dot{\xi}(t)$ and $\dddot{\xi}(t)$ are derivatives of the output variable of the filter (15). Triple differentiation of $\xi(t)$ gives $-\Omega^2 \dot{\xi}(t) + \Omega^2 \varepsilon_\xi(t) + \dddot{\varepsilon}_\xi(t)$, in which $\varepsilon_\xi(t) = \Omega^2 \dot{\varepsilon}_\xi(t) + \dddot{\varepsilon}_\xi(t)$ is the exponential damped function with exponential damped derivatives defined by non-zero initial conditions [14]; $\Theta = -\Omega^2$ is a constant parameter. The updated law for the identification of Θ, including the frequency Ω [8], is as follows:

$$\begin{cases} \hat{\Omega} = \sqrt{|\Theta|} \\ \hat{\Theta} = \chi + \gamma_3 \dot{\xi} \dddot{\xi} \\ \dot{\chi} = -\gamma_3 \dot{\xi}^2 \hat{\Theta} - \gamma_3 \dddot{\xi}^2 \end{cases} \tag{17}$$

where $\hat{\Omega}$ is an estimated frequency Ω and $\hat{\Theta}$ is an estimated unknown parameter Θ. The estimated error $\tilde{\Omega} = \Omega - \hat{\Omega}$ is guaranteed to converge to zero and is bounded by a decaying exponent $|\tilde{\Omega}(t)| \le \sqrt{|\tilde{\Theta}(t)|} \le \rho_0 e^{-\beta_0 t}$, where ρ_0 and β_0 are positive numbers [14]. The derivative of the estimated error $\tilde{\Theta} = \Theta - \hat{\Theta}$ can be proved with a positive constant γ_3 as follows:

$$\begin{aligned} \dot{\tilde{\Theta}}(t) &= \dot{\Theta} - \dot{\hat{\Theta}}(t) \\ &= -\dot{\chi}(t) - \gamma_3 \dddot{\xi}^2(t) - \gamma_3 \dot{\xi}(t) \dddot{\xi}(t) \\ &= -(-\gamma_3 \dot{\xi}^2(t) \hat{\Theta}(t) - \gamma_3 \dddot{\xi}^2(t)) - \gamma_3 \dddot{\xi}^2(t) - \gamma_3 \dot{\xi}(t) \dddot{\xi}(t) \\ &= \gamma_3 \dot{\xi}^2(t) \hat{\Theta}(t) - \gamma_3 \dot{\xi}^2(t) \Theta - \gamma_3 \dot{\xi}(t) \varepsilon_\xi(t) \\ &= -\gamma_3 \dot{\xi}^2(t) \tilde{\Theta}(t) - \gamma_3 \dot{\xi}(t) \varepsilon_\xi(t) \end{aligned} \tag{18}$$

The P.D. Lyapunov function is $V_2 = \frac{1}{2} \tilde{\Theta}^T \Gamma_1 \tilde{\Theta}$, where Γ_1 is a symmetric P.D. matrix. Using the result in Eq. (18), the following can be obtained:

$$\begin{aligned} \dot{V}_2 &= \tilde{\Theta}^T \Gamma_1 \dot{\tilde{\Theta}} = \tilde{\Theta}^T \Gamma_1 (-\gamma_3 \dot{\xi}^2 \tilde{\Theta}) - \gamma_3 \Gamma_1 \dot{\xi} \tilde{\Theta} \varepsilon_\xi \\ &= -\gamma_3 \dot{\xi}^2 V_2 + \frac{1}{2} \gamma_3 \Gamma_1 \varepsilon_\xi^2 \le 0 \end{aligned} \tag{19}$$

It is clear from Eq. (19) that   is a non-increasing function and, hence, V_2 is bounded. According to Barbalat's Lemma, $V_2 \to 0$ as $t \to \infty$, which also leads to $\tilde{\Omega} \to 0$. Consequently, the updated law in Eq. (17) is proven to estimate the frequency $\hat{\Omega} \to \Omega$ of the sinusoidal signal.

ESTIMATION FOR OFFSET, AMPLITUDE, AND PHASE

To estimate the rest of the parameters, the disturbance is calculated as follows:

$$d(t) = \theta^T \varphi(t) \tag{20}$$

where $\theta = \begin{bmatrix} F_o & a & b \end{bmatrix}^T$ is a vector of unknown constants and $\varphi(t) = \begin{bmatrix} 1 & \cos(\Omega t) & \sin(\Omega t) \end{bmatrix}^T$ is the regression vector [9]. Replacing into Eq. (14) gives

$$\dot{V}_1 = -\gamma_1 x_1^2 - \gamma_2 z_2^2 + z_2(\theta^T \varphi - \hat{\theta}^T \varphi) = -\gamma_1 x_1^2 - \gamma_2 z_2^2 + z_2 \tilde{\theta}^T \varphi \tag{21}$$

where $\tilde{\theta} = \theta - \hat{\theta}$ is the estimated error. With a P.D Lyapunov function $V_3 = V_1 + \frac{1}{2} \tilde{\theta}^T \Gamma_2^{-1} \tilde{\theta}$, where Γ_2 is a symmetric P.D matrix, the derivative $\dot{V}_3$ is given as:

$$\begin{aligned} \dot{V}_3 &= \dot{V}_1 + \tilde{\theta}^T \Gamma_2^{-1} \dot{\tilde{\theta}} = -\gamma_1 x_1^2 - \gamma_2 z_2^2 + z_2 \tilde{\theta}^T \varphi - \tilde{\theta}^T \Gamma_2^{-1} \dot{\hat{\theta}} \\ &= -\gamma_1 x_1^2 - \gamma_2 z_2^2 + \tilde{\theta}^T (\varphi z_2 - \Gamma_2^{-1} \dot{\hat{\theta}}) \end{aligned} \tag{22}$$

To make $\dot{V}_3$ an N.D. function, the update law should be chosen as follows:

$$\dot{\hat{\theta}} = \Gamma_2 \varphi z_2 \tag{23}$$

Finally, with the chosen update law, $\dot{V}_3 = -\gamma_1 x_1^2 - \gamma_2 z_2^2$ is an non-increasing function and V_3 and V_1 are bounded, hence $x_1 \to 0$ and $\hat{\theta} \to \theta$ as $t \to \infty$. To sum up, the necessary parameters for estimating sinusoidal disturbance and controller have been explained. In the next section, simulation results illustrate the system's dynamic behaviour under backstepping control with an adaptive mechanism, as well as the estimation process, to formulate the external disturbance.

NON-PERIODIC ROLL PREDICTION USING RC

In contrast to conventional RNN, only the readout weight is trained. The input weight (W_{in}), feedback weight (W_{fb}), and adjacency matrix (W_{res}) are fixed and chosen randomly. In some simple applications, where feedback response is not required, W_{fb} can be omitted. Based on similar effects on reservoirs, W_{in} and W_{fb} are primarily constructed in the same way. Both input and feedback responses can be used to generate output [15]. For a reservoir with N neurons, the structure of a general ESN, having N reservoir states, is illustrated in Fig. 1. The linear mapping input-output at a perceptron is presented in Fig. 1.
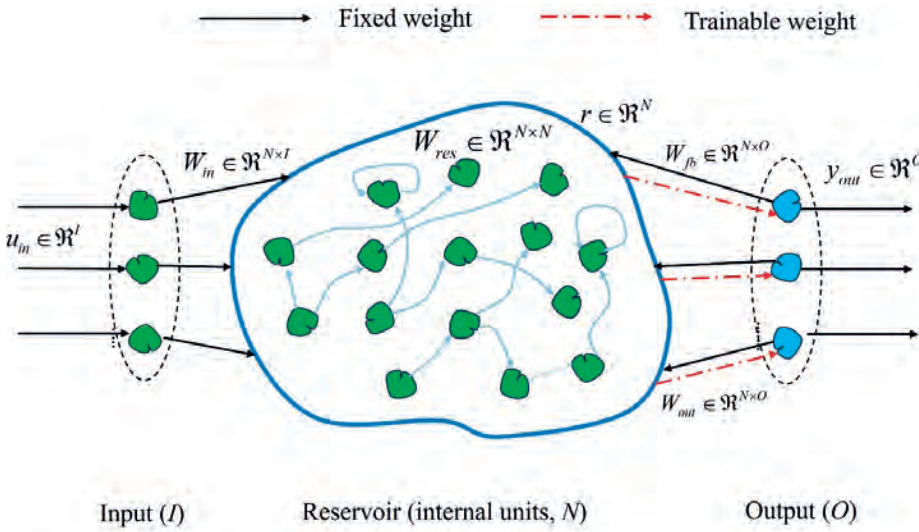
Fig. 1. Generic sketch of the RC framework

According to [15], the complete form of the updated equation for the reservoir state vector $r(n)$ is defined as follows:

$$\tilde{r}(n) = \tanh\left(W_{in}\begin{bmatrix} b_{in} \\ u_{in}(n) \end{bmatrix} + W_{res}r(n) + W_{fb}y_{out}(n-1)\right) \quad (24)$$

$$r(n) = (1-\alpha)r(n-1) + \alpha\tilde{r}(n) \quad (25)$$

where $u_{in}(n) \in \mathfrak{R}^I$ is the input fed to the reservoir at time step n ($n = 1,...,T$); T is a data point in the training dataset; b_{in} is the bias of the reservoir's input; $r(n) \in \mathfrak{R}^N$ is a vector of a reservoir neuron; $\tilde{r}(n)$ is its updated value; and $y_{out}(n) \in \mathfrak{R}^O$ is a vector of network outputs [13]. Weight matrices W_{in}, W_{res}, and W_{fb} are defined as the input weight matrix, the adjacency matrix describing the connection of the nodes in the reservoir, and the feedback weight matrix from the output back to the reservoir, respectively. α is the leaking rate ($0 \le \alpha \le 1$). Without the leaking term, $\tilde{r}(n) \equiv r(n)$

for the case where $\alpha = 1$, $f(x) = \tanh(x)$ is the activation function. The weighted sum of the input states is then fed through an activation function to give the final output. The most basic activation function is the step function. However, smooth (sigmoid) functions are mostly preferred, such as the hyperbolic tangent function $\tanh(x)$. Eqs. (24) and (25) indicate that the reservoir state $r(n)$ will be updated based on the current input $u_{in}(n)$ and the feedback from the previous sample $y_{out}(n-1)$. The feedback term can be omitted in some tasks, where the feedback state is unnecessary. The output state $y_{out}(n)$ of the reservoir at the sampling point can be calculated from the linear combination between the reservoir state and input state, as below [15]:

$$y_{out}(n) = W_{out}\begin{bmatrix} b_{out,} \\ u_{in}(n) \\ r(n) \end{bmatrix} \quad (26)$$

where W_{out} is the weight matrix from the reservoir to the output and b_{out} is the bias of the reservoir's output. In the training procedure, the input data is the reference data (teacher data) and the actual output of the reservoir is replaced by the desired output [15]. Within a training duration of samples, all input and output data are collected into matrices $Y^{(N \times T)}$ and $X^{(N \times T)}$, by concatenating T columns. Regarding Eq. (26), the linear relation between Y and X can be written in matrix form, as follows:

$$Y = W_{out}X \quad (27)$$

At the end of the training phase, the trained weight matrix W_{out} can be analytically computed using ridge regression.

$$W_{out} = YX^T(XX^T + \nu I)^{-1} \quad (28)$$

where ν is the regularisation constant added to avoid overfitting and I is the identity matrix. After the training phase, the output weight W_{out} is computed and can be used for continuous computation. The actual output of the iteration can be reapplied as input for the next iteration. The teacher data is now unnecessary because the reservoir computer can generate prediction data. As presented in Eq. (26), the actual output of the reservoir can be obtained.

SIMULATION RESULTS

DYNAMIC ANALYSIS OF NON-PERIODIC ROLL MOTIONS

In this section, finding the chaos using dynamic theory, stabilisation, and the parametric identification of unknown periodic disturbances are discussed in sequence. Numerical simulations are performed to reveal the effectiveness of the proposed mechanism. The main parameters of the chosen model, from a marine vessel, [7] show strong nonlinear characteristics such as chaos, limit cycles, and resonance under periodic disturbances [16]. For the numerical simulation, the initial condition (IC) of the roll dynamics is = [0.5 (rad) 0.2 (rad/s)].

First, we analysed the non-periodic roll motions before parametric estimation and stabilisation. The bifurcation diagram easily recognises this phenomenon, representing the qualitatively sudden change as a varied parameter. When a small perturbation causes the qualitative responses in the system, it is regarded as unstable, whereas the opposite case is stable. This roll model shows rich dynamic behaviours, depending on the initial conditions. For example, a strange attractor exhibits sensitivity to initial conditions.
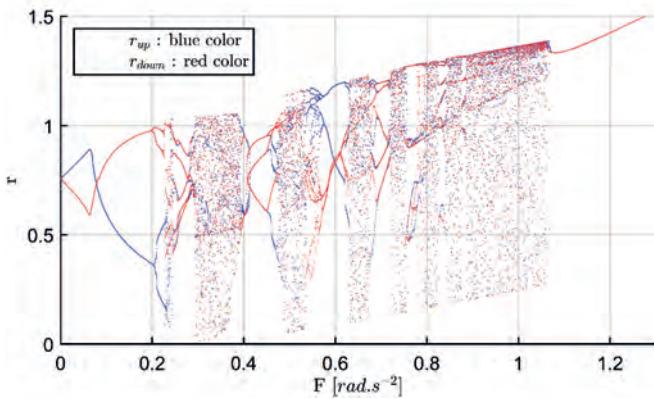
The ramp-up and ramp-down parts of the graph are necessary for observing the bistable region [17]. Fig. 2 shows the stable and unstable rolling motions, based on the second iterative method, where $r = (\sqrt{x_1^2 + x_2^2})$ is the distance from the origin in the Poincare map [18]. The ramp-up (r_{up}, in blue) and ramp-down (r_{down}, in red) parts enable checking of the bistable region. F is the forcing amplitude of wave excitations, with respect to roll mode after dividing inertia terms. A ship's motion is stable, with periodic responses, until F reaches a value of 0.2. However, the branches in the diagram start to split (bifurcate) into two new branches from the point $F = 0.2$, and the ship becomes unstable. Such unstable regions are more dominant, as the forcing amplitude reaches 1. Period-doubling routes to chaos and period-undoubling routes to single branches are clearly observed when the F increases. With a slight rise in forcing amplitude, the periodic windows, which are stable regions, can be seen among the chaotic clouds of dots.

Fig. 3(a) illustrates the Lyapunov exponents (LEs) of the uncontrolled systems, demonstrating a chaos system. It is a measure of predictability and sensitivity for controlling parameter changes. The exponential growth in LE_i can be estimated as follows:

$$\left\| \Delta_i(t) \right\|_2 \approx \left\| \Delta_i(0) \right\|_2 e^{LE_i t} \, , 1 \le i \le n \qquad (29)$$

where $\left\| \Delta_i(0) \right\|_2$ denotes the initial separation, with a chaotic motion of $LE_i > 0$ making behaviour *unpredictable*, whereas $LE_i \le 0$ for regular motion. The stretching and contracting of attractors can be defined with LEs, whose positive values signify chaos [19]. The LE measures the mean rate of exponential divergence of nearby trajectories, which gives information on the growth rate of IC. The positive LEs (LE_1, blue line) show that the system is sensitive to IC and their trajectories diverge with time, while negative LEs (LE_2, red line) indicate a tendency for convergence. A positive LE usually indicates that the system is chaotic. The larger the exponent, the more unstable the system. The negative LEs mean that the system is stable. The negative LEs are characteristic of dissipative systems, such that the roll system exhibits asymptotic stability; the more negative the exponent, the greater the stability [17].
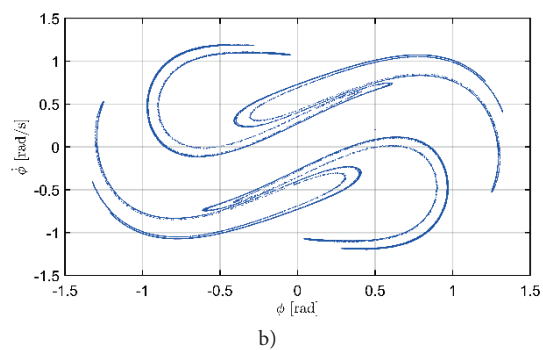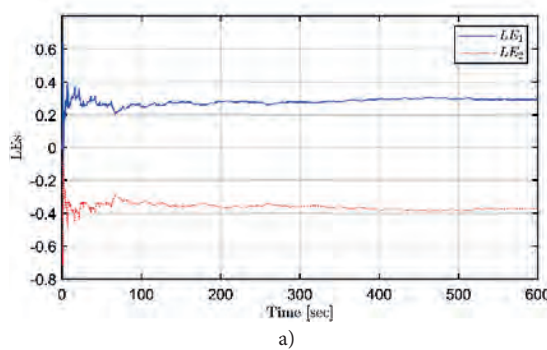

Fig. 2. Bifurcation diagram using the second iterative method

a)   b)

Fig. 3. Dynamic analysis of the uncontrolled system in the case of IC [0.5 (rad) 0.2(rad/s)]: (a) Lyapunov exponents; (b) Poincare section

Fig. 3(b) shows where the Poincare section shows a deterministic system's uncontrolled roll, with no random or noisy inputs; it appears to be non-periodic. The main parameters are adopted in a marine model [7]. The Poincare map reduces the n-dimensional flow to a $n-1$ dimensional map. All trajectories of an n-dimensional system start on the $n-1$ dimensional surface of a section flowing through it. Such reduced dimensionality makes it possible to preserve periodic and quasi-periodic orbits. To make an autonomous flow in a torus, a third value $\theta = \Omega t$ can be considered from Eq. (6) without control. A trajectory flowing around a torus with a period ($T = 2\pi / \Omega$) leads to the Poincare mapping of a $\theta = \theta_0$ plane. Picking up a cross-section of roll angle and rate, the Poincare map is mainly varied according to the strength of the forcing function. The manifolds become tangential and intersect transversely when F increases. If a trajectory in the phase plane intersects itself repeatedly, then a strange attractor and fractals may be observed in the roll dynamics [20-22].

PARAMETRIC IDENTIFICATION OF PERIODIC DISTURBANCES

Next, the simulations for the proposed backstepping control are conducted. The filter and controller design parameters are set as $(\lambda_0, \lambda_1, \lambda_2, \gamma_1, \gamma_2, \gamma_3) = (0.15, 2, 8, 5, 5, 2.5)$. The updated rate matrix is chosen as $\Gamma_2 = diag(2, 1.2, 1.2)$ and the IC is $(\hat{F}_o(0), a(0), b(0), \Omega(0)) = (0.2, 0.3, 0.1, 0)$. Figs. 4 and 5 demonstrate the estimation process for the frequency, offset, amplitude, and phase, respectively. In contrast, Fig. 5 (a) verifies a combination of the above results to form a complete estimation for the sinusoidal disturbance. All parameters of periodic disturbances can be precisely estimated. Suppression of the roll angle and rate is achieved using the backstepping control, as seen in Figs. 5(b) and 5(c). Finally, filtered signals are illustrated in Fig. 5(d), according to the updated law in Eq. (17).
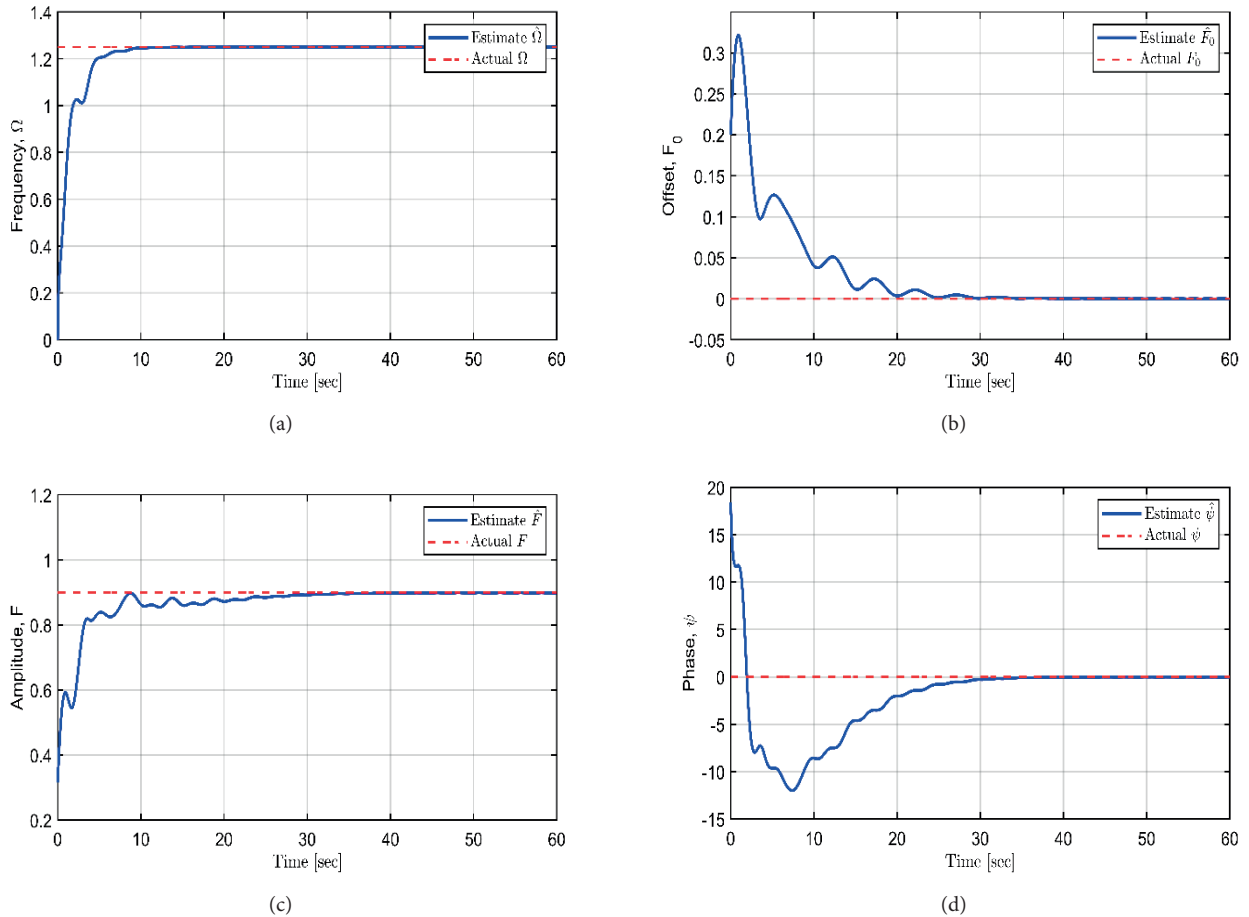

(a)

(b)

(c)

(d)

Fig. 4. Test results of estimation (1): (a) frequency; (b) offset; (c) amplitude; (d) phase
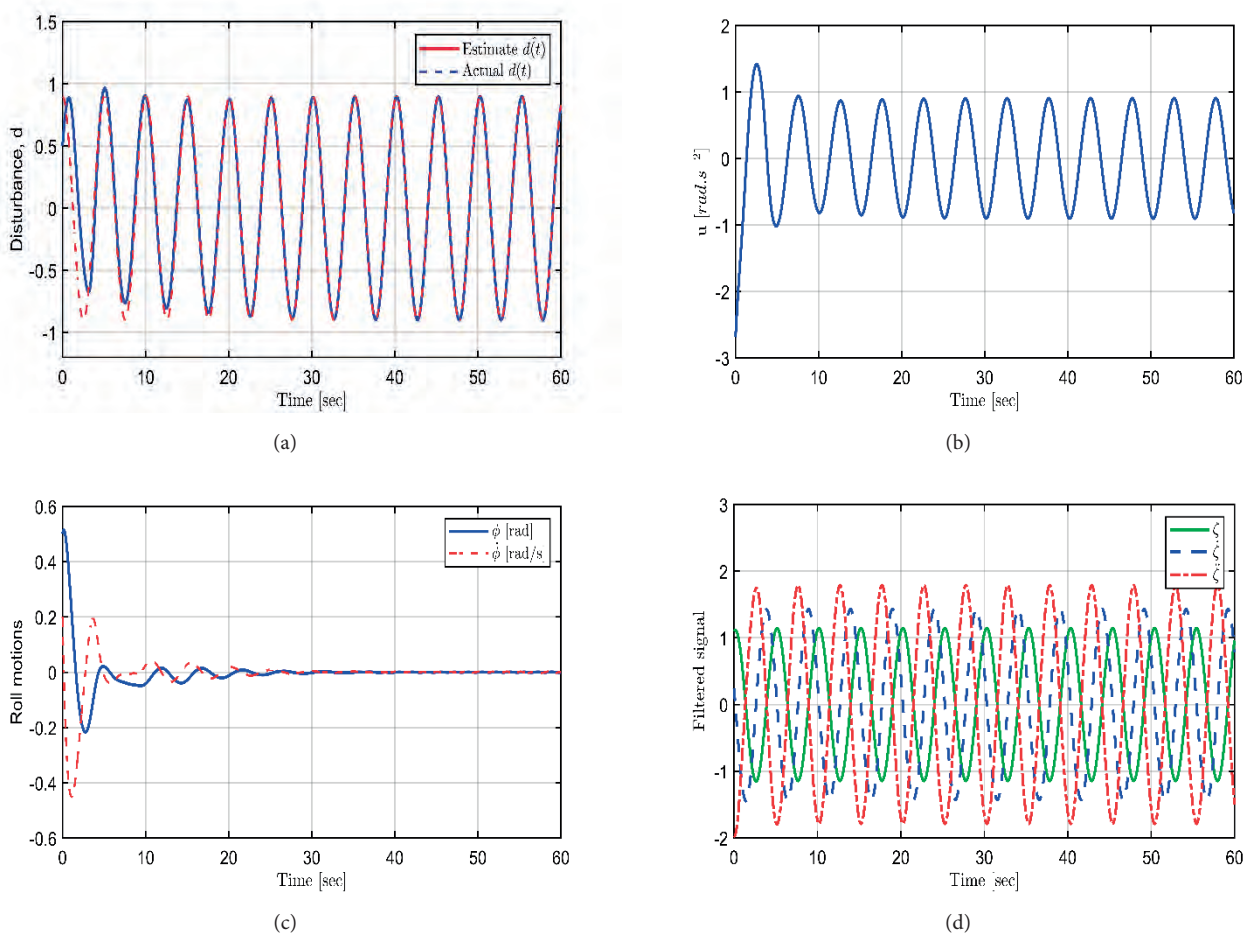
Fig. 5. Test results of estimation (2): (a) periodic disturbances; (b) control inputs; (c) suppression of two states; (d) filtered signals

SHIP ROLL PREDICTION USING RC

Finally, the non-periodic rolling motions are predicted via RC. Such an ESN algorithm is used to forecast the reference data of roll angle and roll rate for the training and prediction processes of the reservoir. After the initial input weight (W_{in}) and feedback weight (W_{fb}) are fixed, the predicted process is performed from the computation of the trained reservoir. In fact, the prediction performance strongly depends on the parameter values, as listed in Table 1. A reservoir size (N), related to the memory capacity, is selected as $N = 600$, where σ is a hyper-parameter for adjusting the performance. The input range $[-\sigma, \sigma]$ indicates the dispersion level of components in the weight matrices (W_{in} , W_{fb}). The adjustment of the leaking rate (α) indicates the level of dependence of the network on past information. The lower the α value, the more dependent it is on past information. The spectral radius (ρ) is related to the magnitude of the largest eigenvalue of internal weight (W_{res}) and performance. As α increases, the wider it spreads on the weight matrices. The author decided that α should not be too low because it will inflict an amplitude value on input and feedback responses.

Tab. 1. Main parameter values for the prediction model

Reservoir size (N)	Hyper-parameter (σ)	Leaking rate (α)	Regularisation coefficient (ν)	Spectral radius (ρ)
600	0.5	0.1	10^{-8}	0.75

The prediction performance of *quantitative* and qualitative measures, such as error criteria and non-periodic orbits in future states, is presented. At first, the mean squared error (MSE) is employed to evaluate the prediction performance, which measures the average of the squares of the errors. It shows a positive value that decreases, as the error approaches zero, and is defined as follows:

$$\text{MSE} = \frac{1}{n} \sum_{n=1}^{n} (Y_T - \hat{Y}_T)^2 \tag{30}$$

where Y_T and $\hat{Y}_T$ describe the actual and predicted values of roll responses in the time period, respectively.

The numerical tests were conducted based on several scenarios: Case 1 ($T_T = 160$, $P_T = 40$), Case 2 ($T_T = 200$, $T_P = 400$), Case 3 ($T_T = 200$, $P_T = 800$), and Case 4 ($T_T = 400$, $P_T = 800$), where T_T and P_T mean the times of training and prediction, as listed in Table 2. The indices show that the results of Case 1, Case 2, and Case 4 are better than Case 3. When T_P increases, the values of MSE increase as well, and prediction performance is degraded over time. Then, a proper T_P should be adjusted accordingly. The ratio value of $T_T / P_T = 0.5$ is necessary for this simulation. Interestingly, the results of RC slightly vary at every simulation. The test results of each case are changeable, according to the reservoir size or the other parameters in Table 1.

Tab. 2. Prediction accuracies using performance index (MSE)

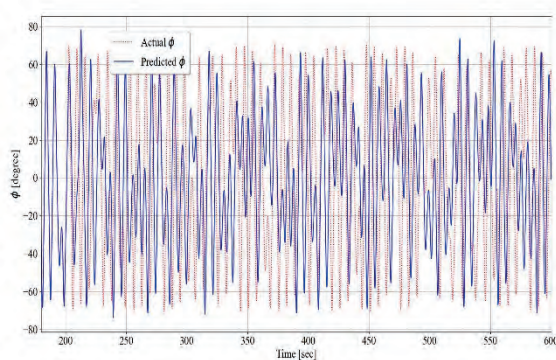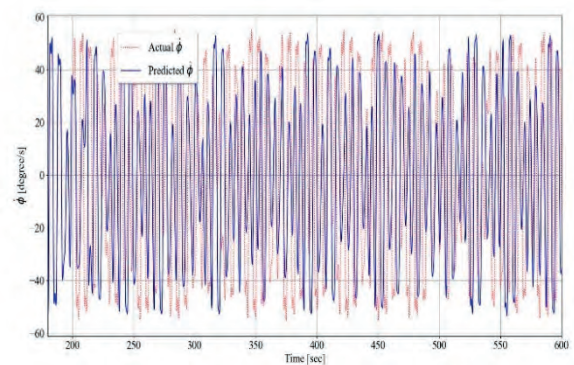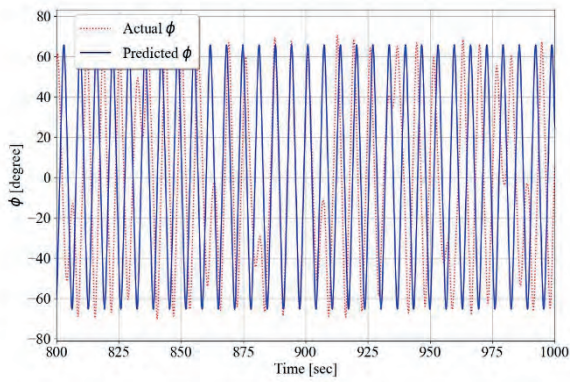| States	Case 1 $(T_T / P_T = 4)$		Case 2 $(T_T / P_T = 0.5)$		Case 3 $(T_T / P_T = 0.25)$		Case 4 $(T_T / P_T = 0.5)$	
	T_T	P_T	T_T	P_T	T_T	P_T	T_T	P_T
	160 s	40 s	200 s	400 s	200 s	800 s	400 s	800 s
$x_1(\phi)$	0.3336		0.8659		1.0768		0.8912	
$x_2(\dot{\phi})$	0.2342		0.6809		0.8946		0.6383	
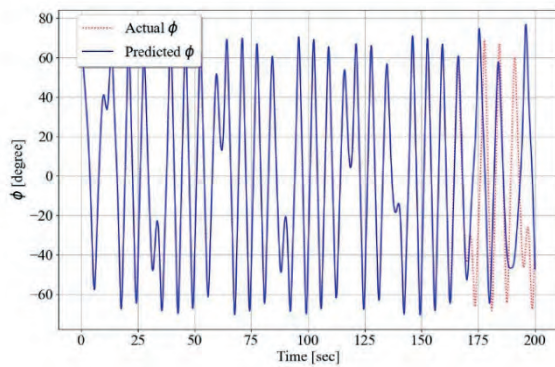
(a)
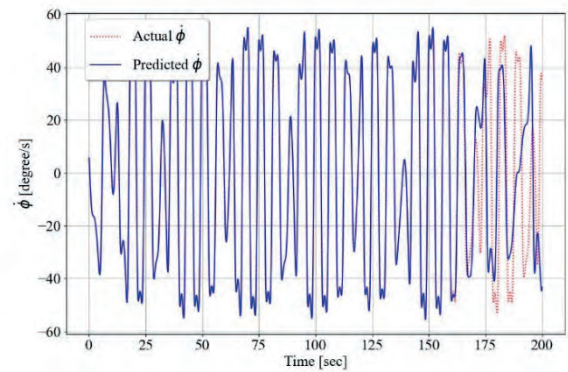
(b)

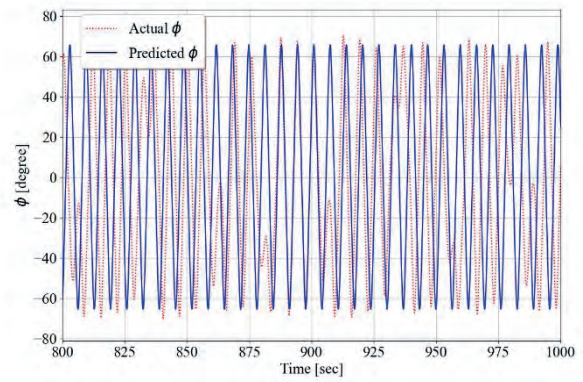Fig. 6. Prediction results (Case 1): (a) roll angle; (b) roll rate

(a)

(b)

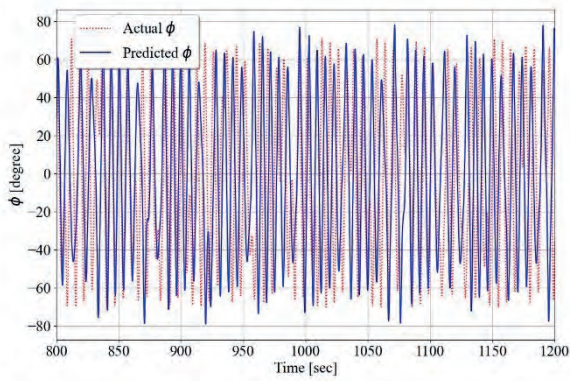Fig. 7. Prediction results (Case 2): (a) roll angle; (b) roll rate
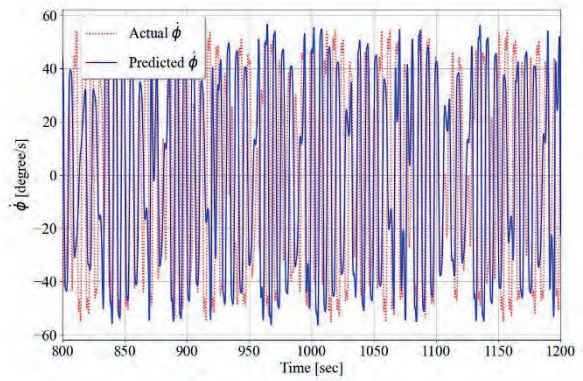
Fig. 8. Prediction results (Case 3): (a) roll angle; (b) roll rate

Fig. 9. Prediction results (Case 4): (a) roll angle; (b) roll rate

The main purpose of the RC is to predict chaotic time series behaviours. Figs. 6 to 9 depict the qualitative features of prediction results based on the training time T_T of 160-400 seconds. Then, the model performance is demonstrated by increasing the prediction time P_T by 40-800 seconds. Figs. 6, 7, and 9 show that the non-periodic pattern is clear for cases where $T_T > P_T$ and $T_T < P_T$. However, chaotic time series prediction is obscure, due to the insufficient T_T, as seen in Fig. 8. Chaotic features become evident in Fig. 9, by increasing T_T. Thus, prediction performance can be secured in the case of $T_T / P_T \geq 0.5$, by adjusting the corresponding T_T and P_T. As a result, the RC process shows good performance, even for chaotic time series prediction in future states, although it lacks predictability [6].

CONCLUSIONS

One can easily imagine that the marine environment is not easy for humans and marine vessels to deal with. This paper has investigated two topics: how to estimate the parameters of unknown ocean disturbances and how to control a ship's dynamic behaviour in future states. The rolling behaviour of marine vessels shows non-periodic responses, as well as regular responses. Sometimes, the complicated rolling motions are demonstrated by strong nonlinearities or forcing amplitudes of extreme wave excitation. Specifically, the complex behaviours of a rolling system are investigated by nonlinear analyses, such as bifurcation diagrams, the Lyapunov exponent (LE), and Poincaré maps. The chaos is not a casual phenomenon but, rather, it yields particular responses. It is an aperiodic, long-term motion that exhibits sensitive dependence on the initial conditions in a deterministic system. The nonlinear rolling motion shows a strange attractor, depending on the initial conditions. The

second iterative method of the bifurcation diagram displays the unstable qualitative responses in the ship's roll due to slight changes in the parameters, such as the initial conditions or forcing amplitudes. Based on the magnitude of the wave excitations, rich dynamic responses can be observed, such as periodic (stable, regular) routes to chaos (reverse doubling), and chaos at the end. In fact, a ship under excessive rolling motions may result in a capsized state with no other recovery oscillations until it is in an upright position. Since there is no response amplitude operator (RAO), including wave height, in this paper, it is a limitation that marine vessels do not recognise the precise timing of chaos or capsize in sea states. It is difficult for ships' crews to deal with the abrupt changes in the rolling motions.

Therefore, this paper has investigated rolling motion predictions for marine vessels with machine-learning methods and parameter estimation of unknown disturbances. All parameters, such as frequency, offset, amplitude, and phase, are precisely estimated based on the adaptive mechanism without any observers. The linear second-order filters and parameter estimation errors are employed to achieve global exponential convergence. Also, the backstepping method is realised, to regulate the roll angle and rate, in the case of severe disturbances to marine vessels. Moreover, the RC process revealed its predictive performance in terms of the future states' chaotic time series behaviours. This may help to support the lack of predictability by LEs [6]. Unfortunately, prediction performance is highly dependent on the parameter values selected by the designer's empirical trials. Interestingly, the results of RC vary slightly in every simulation. According to the reservoir size, practitioners might find the optimum values of parameters. However, the method presented may help them obtain a satisfactory conclusion. Insufficient training time causes the obscure prediction of chaotic orbits. Thus, prediction criteria and the prediction and training time ratio are necessary. This paper suggests a ratio value of greater than 0.5 but it has a limitation of slow convergence in transient performance; however, it shows less oscillation due to the second-order filtered signals [9]. Finding the proper values to adjust to fast convergence speed and transient performance is necessary. To make a safe and robust system of marine vessels under severe sea environments, an adversarial attack might be considered, based on adaptive control with machine learning skills or quantum RC in future research.

ACKNOWLEDGEMENT

REFERENCES

1. E. Ott, C. Grebogi, J.A. Yorke, 'Controlling chaos', Phys. Rev. Lett. 1990, 64, 1196–1199, DOI: 10.1103/PhysRevLett.64.1196.

2. Y. Tang, J. Kurths, W. Lin, E. Ott, and L. Kocarev, 'Introduction to Focus Issue: When machine learning meets complex systems: Networks, chaos, and nonlinear dynamics', Chaos 2020, 30 (6), 063151, DOI: 10.1063/5.0016505.

3. H. Jaeger and H. Haas, 'Harnessing nonlinearity: Predicting chaotic systems and saving energy in wireless communication', Science 2004, 304 (5667), 78–80, DOI: 10.1126/science.109127.

4. Y. LeCun, Y. Bengio, and G. Hinton, 'Deep learning', Nature 2015, 521, 436–444. https://doi.org/10.1038/nature14539.

5. A.A. Ferreira, T.B. Ludermir, and R.R.B. De Aquino, 'An approach to reservoir computing design and training', Expert Syst. Appl. 2013, 40(10), 4172-4182, DOI: 10.1016/j.eswa.2013.01.029.

6. G. Boffetta, M. Cencini, M. Falcioni, and A. Vulpiani, 'Predictability: A way to characterize complexity', Phys. Rep. 2002, 356, 367–474, DOI: 10.1016/S0370-1573(01)00025-4.

7. S.D. Lee, B.D.H. Phuc, X. Xu, and S.S. You, 'Roll suppression of marine vessels using adaptive super-twisting sliding mode control synthesis', Ocean. Eng. 2020, 195, 106724, DOI: 10.1016/j.oceaneng.2019.106724.

8. A.A. Pyrkin, A.A. Bobtsov, S.A. Kolyubin and A.A. Vedyakov, 'Precise frequency estimator for noised periodical signals', 2012 IEEE International Conference on Control Applications. 2012, 92-97, DOI: 10.1109/CCA.2012.6402392.

9. N. Jing, Y. Juan, W. Jing and G. Yu, 'Adaptive parameter identification of sinusoidal signals', 2013 IFAC Conference on Intelligent Control and Automation Science ICONS, 2013, 624-629, DOI: 10.3182/20130902-3-CN-3020.00096.

10. M. Hou, 'Parameter identification of sinusoids', IEEE Transactions on Automatic Control. 2012, 57(2), 467–472, **DOI:** 10.1109/TAC.2011.2164736.

11. J. Na, J. Yang, X. Wu, and Y. Guo, 'Robust adaptive parameter estimation of sinusoidal signals', Automatica. 2015, 53, 376-384, DOI:10.1016/j.automatica.2015.01.019.

12. V. Adetola and M. Guay, 'Performance Improvement in Adaptive Control of Linearly Parameterized Nonlinear Systems', IEEE Transactions on Automatic Control. 2010, 55(9), 2182-2186, **DOI:** 10.1109/TAC.2010.2052149.

13. S.D. Lee, Y.S. Song, D.H. Kim, and M.R. Kang, 'Path following control of an underactuated catamaran for recovery maneuvers', Sensors. 2022, 22, 2233, doi.org/10.3390/s22062233.

14. A.A. Pyrkin, 'Adaptive algorithm to compensate parametrically uncertain biased disturbance of a linear plant with delay in the control channel', Autom Remote Control. 2010, 71, 1562–1577.

15. M. Lukoševičius, 'A Practical Guide to Applying Echo State Networks. In: Montavon, G., Orr, G.B., Müller, KR. (eds) Neural Networks: Tricks of the Trade. Lecture Notes in Computer Science', 2012, vol 7700. Springer, Berlin, Heidelberg. https://doi.org/10.1007/978-3-642-35289-8_36.

16. S.D. Lee, S.S. You, X. Xu, and T.N. Cuong, 'Active control synthesis of nonlinear pitch-roll motions for marine vessels'. Ocean Eng. 2021, 221, 108537, DOI: 10.1016/j.oceaneng.2020.108537.

17. S. Lynch, 'Poincaré Maps and Nonautonomous Systems in the Plane. In: Dynamical Systems with Applications using MATLAB®', 2014, Birkhäuser, Cham, DOI: 10.1007/978-3-319-06820-6_15.

18. E. Ott, 'Chaos in Dynamical Systems (2nd ed.)', Cambridge: Cambridge University Press. 2002. DOI: 10.1017/CBO9780511803260.

19. S. Lynch, 'Electromagnetic Waves and Optical Resonators. In: Dynamical Systems with Applications using MATLAB®', 2014, Birkhäuser, Cham, DOI: 10.1007/978-3-319-06820-6_5.

20. K.K. Dey and G.A. Sekh, 'Effects of Random Excitations on the Dynamical Response of Duffing Systems', J Stat Phys. 2021, 182, 18, DOI: 10.1007/s10955-020-02694-x.

21. B.S. Ahmed, 'A practical test for noisy chaotic dynamics', SoftwareX. 2015, 3–4, 1-5, DOI: 10.1016/j.softx.2015.08.002.

22. J.J. Bramburger and J. Nathan Kutz, 'Poincaré maps for multiscale physics discovery and nonlinear Floquet theory', Physica D: Nonlinear Phenomena. 2020, 408,132479, DOI: 10.1016/j.physd.2020.132479.